A partitioned resolution for concurrent fluid flow and stress analysis during solidification: application to steel ingot casting

Michel Bellet, Okba Boughanmi, Grégory Fidel

▶ **To cite this version:**

HAL Id: hal-00714046

A partitioned resolution for concurrent fluid flow and stress analysis during solidification: application to ingot casting

Michel Bellet, Okba Boughanmi, Grégory Fidel

MINES ParisTech - CEMEF, CNRS UMR 7635, Sophia Antipolis, France

michel.bellet@mines-paristech.fr

Abstract. In simulation of solidification processes, an open issue is the concurrent modelling of fluid flow and solid mechanics. This is critical for the prediction of cracks formed in solidified regions during the filling stage of ingot casting, or in the mould during continuous casting. The proposed approach consists of a partitioned two-step resolution strategy.

1. Introduction

When modelling casting processes, one of the critical issue is to achieve a concurrent computation of fluid flow (ingot mould filling, thermal convection, nozzle jet in continuous casting) and solid mechanics (stress-strain in solidified regions). This is of crucial importance for the prediction of surface or sub-surface cracks that may initiate in solidified regions during the filling stage of ingot casting, or during continuous casting. The current state-of-the-art consists in separating the analysis in two distinct stages: fluid flow using CFD codes and stress-strain analysis using structural codes. This induces several drawbacks regarding practical use and computational efficiency. A monolithic formulation, treating the Fluid-Solid Interaction (FSI) could be seen as a possible alternative, but is not adapted to the context of solidification, because of huge differences between liquid viscosity and solid consistency. It is then preferable to consider this FSI problem as a weak interaction problem, for which a partitioned formulation is more efficient than a monolithic one. Therefore, a two-step resolution strategy combining fluid flow and solid mechanics has been developed:

- In a first step, a solid-oriented resolution is performed, in which the liquid is modelled using an arbitrary high viscosity. From this first resolution we get the velocity field in solidified regions, and associated strains and stresses. This resolution is highly non-linear due to the elastic-viscoplastic constitutive models used for the solid material.
- A second step consists of a liquid-oriented resolution: Navier-Stokes equations, including buoyancy, and Darcy contributions in mushy zone, are considered. This resolution can be linearized and therefore is computationally less demanding than the first one.

Both resolutions are performed using a level set formulation to track the evolution of the interface air/metal. This approach is applied to the continuous simulation of the filling and cooling of a parallelepipedic ingot, showing the ability to predict stress and strain fields during the filling stage which cannot be achieved by standard casting simulation codes.

2. Two-step coupled formulation for mechanical modelling

The main limitation of a monolithic formulation is its inability to consider concurrently a low viscous liquid and an elastic-viscoplastic solid. To overcome this limitation, a 2-step resolution strategy has

been developed, which consists in dividing the mechanical problem into two coupled sub-problems, which are detailed in the next sections:

- a solid-oriented resolution, from which velocities, stresses and distortions are calculated in the solidified regions;
- a liquid-oriented resolution which gives access to velocity and pressure fields in the liquid regions and in the air.

2.1. Step I: solid-oriented resolution

2.1.1. *Constitutive equations.* In the first step, the approach proposed in [1][2] is applied. A thermo-elastic-viscoplastic (TEVP) model is used for the solid state. A thermo-viscoplastic (TVP) model is used to model the behaviour of the metal both in the mushy and the liquid states. The mushy metal is considered as an homogenized non-Newtonian fluid, in which the strain-rate sensitivity is continuously increasing with the liquid fraction. At liquidus temperature, the behaviour tends to the Newtonian model, which is used in the fully liquid state. However, in Step I, the liquid is modelled using an arbitrary high value for the viscosity (typically 1 to 100 Pa s instead of nominal values around 10^{-3} Pa s). TEVP and TVP behaviour models are distinguished by a critical transition temperature T_c chosen equal to the solidus temperature.

2.1.2. *Equations solved.* The weak form of the following momentum and mass conservation equations are solved by a finite element method [1]:

$$\begin{cases} \nabla \cdot \mathbf{s} - \nabla p + \rho \mathbf{g} - \rho \dfrac{d\mathbf{v}}{dt} = 0 \\ \nabla \cdot \mathbf{v} - \mathrm{tr}\,\dot{\boldsymbol{\varepsilon}}^{el} - \mathrm{tr}\,\dot{\boldsymbol{\varepsilon}}^{th} = 0 \end{cases} \tag{1}$$

where $\mathbf{s}$ is the deviatoric stress tensor, p the pressure, $\mathbf{g}$ the gravity vector and $\dot{\boldsymbol{\varepsilon}}$ the strain rate tensor. When assembling the stiffness matrix and right hand side to solve the mechanical problem, tetrahedral elements are treated differently according to their average temperature: if it is lower than T_c their behaviour is TEVP, otherwise they are treated using the TVP model. In this latter case, the term $\mathrm{tr}\,\dot{\boldsymbol{\varepsilon}}^{el}$ is absent from the contribution of TVP elements in the weak form of Eq. (1b). The contributions of thermal dilatation and solidification shrinkage are included in the trace of $\dot{\boldsymbol{\varepsilon}}^{th}$, which is written as:

$$\dot{\boldsymbol{\varepsilon}}^{th} = -\frac{1}{3\langle\rho\rangle}\frac{d\langle\rho\rangle}{dt}\mathbf{I} \tag{2}$$

where the average density of the metal is $\langle\rho\rangle = g_s\rho_s + g_l\rho_l$, with ρ_s and ρ_l the densities in the solid state and in the liquid state, respectively. It is assumed that ρ_s and ρ_l depend on temperature, except in the solidification interval where they are constant. Under this assumption, Eq. (1) includes dilatation in the solid and in the liquid states, together with solidification shrinkage in the solidification interval. The velocity and pressure fields deduced from Step I calculation are denoted $\mathbf{v}_{StepI}$ and p_{StepI}, respectively.

2.2. Step II: liquid-oriented resolution

This second step is a fluid-oriented resolution, which is supposed to provide more accurate velocities in mushy and liquid regions. For solid nodes the velocity is imposed to its calculated value in Step I.

2.2.1. *Constitutive equations.* The behaviour of the liquid in Step II is chosen to be Newtonian using the nominal dynamic viscosity in the liquid state ($\sim 10^{-3}$ Pa s). This behaviour is also applied to the liquid phase circulating in the mushy zone, but in this latter case, Darcy terms are used to model the exchange of momentum between the solid and the liquid phase.

2.2.2. *Equations solved*. The equations are issued from the spatial averaging method [6]:

$$\begin{cases} \nabla \cdot \mathbf{s} - \nabla p - \dfrac{\mu_l g_l}{\mathrm{K}}(\mathbf{v} - g_l \mathbf{v}_s) + g_l \rho_l \mathbf{g} - \rho_{l,ref}\left(\dfrac{\partial \mathbf{v}}{\partial t} + (\nabla \mathbf{v})\mathbf{v}\right) = 0 \\ \nabla \cdot \mathbf{v} = -\dfrac{\rho_S - \rho_L}{\rho_L}\dfrac{\partial g_s}{\partial t} - \nabla \cdot (g_s \mathbf{v}_s) \end{cases} \tag{3}$$

In these equations, vector $\mathbf{v}$ denotes the averaged liquid velocity: $\mathbf{v} = g_l \mathbf{v}_l$. The solid velocity $\mathbf{v}_s$ is known from Step I resolution: $\mathbf{v}_s \equiv \mathbf{v}_{\mathrm{StepI}}$. The first equation is obtained after minor adaptations in order to comply with constraints associated with the fluid flow solver. The permeability K is defined by the Carman-Kozeny model, μ_l denotes the liquid dynamic viscosity and the liquid density is defined as $\rho_l = \rho_{l,ref}(1 - \beta_T(T - T_{ref}))$ where β_T is the volumetric thermal expansion coefficient and the reference temperature T_{ref} is taken equal to the liquidus temperature T_L. Eq. (3b) is the global mass balance, issued from the expression of the averaged density in the mushy state: $\langle\rho\rangle = g_s \rho_S + g_l \rho_L$, with ρ_S and ρ_L the densities at solidus and liquidus temperature, respectively. The weak form of Eq. (3) is solved by a stabilized SUPG-PSPG finite element method [8], in which the velocity of solid nodes $(T < T_S)$ is imposed equal to the velocity calculated in Step I resolution: $\mathbf{v} \equiv \mathbf{v}_{\mathrm{StepI}}$. The velocity and pressure fields deduced from Step II calculation are denoted $\mathbf{v}_{\mathrm{StepII}}$ and p_{StepII}, respectively.

3. Free surface modelling

3.1. Level set method
The level set method [7] is used to track the metal/air interface. The level set function α is defined as the signed distance to the interface. By convention, $\alpha < 0$ corresponds to air, $\alpha > 0$ represents the metal, and $\alpha = 0$ the interface. As the only useful information for our computation is the exact zero iso-value position, the signed distance function is truncated and approached by a sinusoidal filter, in order to limit advection calculations around the interface. The modified level set $\phi(\alpha)$ writes [9]:

$$\phi(\alpha) = -\frac{2E}{\pi} \text{ if } \alpha < -E \qquad \phi(\alpha) = \frac{2E}{\pi}\sin\left(\frac{\pi}{2E}\alpha\right) \text{ if } -E < \alpha < E \qquad \phi(\alpha) = \frac{2E}{\pi} \text{ if } E < \alpha \tag{4}$$

where E is a thickness related to the local mesh size h_{msh} ($E = 10$ to $20\ h_{msh}$). In the finite element context, functions α and $\phi(\alpha)$ are P1 fields (nodal fields, linearly interpolated). Knowing the velocity field on the whole computational domain, function ϕ can be updated at each time increment, expressing the motion of the interface, while keeping its metric property (that is $\|\nabla\phi\| = 1$ by the interface $\phi = 0$) by means of a convective reinitialization equation described in [7] and [9]. This transport equation is stabilized with a SUPG (Streamline-Upwind-Petrov-Galerkin) method [5].

3.2. Mixed material properties
In the neighbourhood of the interface, metal and air properties have to be homogenized in order to show a smooth continuous change. The general expression of a mixing law of a generic variable ψ, is:

$$\langle\psi\rangle = \psi_m H(\phi) + \psi_a(1 - H(\phi)) = \psi_a + (\psi_m - \psi_a)H(\phi) \tag{5}$$

where $\langle\psi\rangle$ denotes the mixed variable, ψ_m its value in the metal, and ψ_a its value in the air. $H(\phi)$ is the mixing function, the values of which are in [0,1], and is directly deduced from the level set function ϕ. In the present study, a P0 mixing law is used. On each tetrahedron $(n = 4)$, we have:

$$H_{P0}(\phi) = \sum_n [\phi_n]_+ / \sum_n |\phi_n| \tag{6}$$

4. Solution Strategy
At each time increment, the resolution algorithm is decomposed in eight successive stages:
- 1$^{\text{st}}$ stage. Thermal resolution. The energy equation is solved, providing the temperature distribution in the metal and in the air, and liquid metal fraction. The advection velocity in the

convection term is $\mathbf{v}_{\text{StepII}} - \mathbf{v}_{msh}$ where $\mathbf{v}_{msh}$ denotes the grid velocity. The velocity field $\mathbf{v}_{\text{StepII}}$ calculated at previous time increment is used in the convection term.

- 2nd stage. Optional mechanical resolution. Step I: solid-oriented. The first folder of the momentum resolution consists of the solid-oriented resolution. This step is optional and triggered as soon as the time past since the more recent Step I resolution exceeds the value Δt_{StepI} (obtained below, stage 8). Step I resolution provides velocity and pressure fields on the whole domain: $(\mathbf{v}_{\text{StepI}}, p_{\text{StepI}})$. However, only $\mathbf{v}_{\text{StepI}}$ at nodes belonging to solid-like elements (those treated as EVP) will be used in the follow-up of the resolution scheme. The stress tensor $\boldsymbol{\sigma}$, and the generalized plastic strain $\bar{\varepsilon}$ and strain rate $\dot{\bar{\varepsilon}}$ are calculated in solid-like elements.

- 3rd stage. Mechanical resolution. Step II: liquid-oriented. The second folder of the momentum resolution consists of the fluid-oriented resolution. This resolution provides velocity and pressure fields on the whole domain: $(\mathbf{v}_{\text{StepII}}, p_{\text{StepII}})$. Note that at nodes belonging to solid-like elements, $\mathbf{v}_{\text{StepII}}$ is imposed equal to $\mathbf{v}_{\text{StepI}}$.

- 4th stage. Mesh updating. Nodes belonging to solid-like elements are considered Lagrangian. Their position is updated, provided that a Step I resolution has been performed at the current time increment. Because Δt_{StepI} is the time past since their last update, and $\mathbf{v}_{\text{StepII}} = \mathbf{v}_{\text{StepI}}$ for the considered nodes, the following updating scheme is applied: $\mathbf{x}^{new} = \mathbf{x}^{old} + \Delta t_{\text{StepI}} \mathbf{v}_{\text{StepII}}$. All other nodes are considered Eulerian and then fixed.

- 5th stage. Free surface tracking. The updating of the level set function permits interface tracking. It is achieved by the convection-reinitialization scheme mentioned in Section 3.1. The advection velocity in the convection term is $\mathbf{v}_{\text{StepII}} - \mathbf{v}_{msh}$ where $\mathbf{v}_{msh}$ denotes the grid velocity. For Eulerian nodes, $\mathbf{v}_{msh} = 0$. For Lagrangian nodes, two cases are distinguished:
  - No Step I resolution at the current increment. The Lagrangian nodes of the grid have not been updated: $\mathbf{v}_{msh} = 0$.
  - The Step I resolution has been performed at the current increment. Lagrangian nodes have been just displaced by $\Delta t_{\text{StepI}} \mathbf{v}_{\text{StepII}}$. Consequently, their grid velocity in the level set convection term is taken as: $\mathbf{v}_{msh} = (\Delta t_{\text{StepI}} / \Delta t_{\text{StepII}}) \mathbf{v}_{\text{StepII}}$.

- 6th stage. Updating mixed properties. This step consists in the mixing of material properties, according to the value of the level set function.

- 7th stage. Optional adaptive remeshing. The remeshing is guided by an error estimator of Hessian type, based on interpolation error. Details can be found in [4].

- 8th stage. Time step determination. Time step is adjusted according to the intensity of convection in air and liquid metal. The nominal time step $\Delta t \equiv \Delta t_{\text{StepII}}$ for the next increment is obtained from a CFL condition. In addition, if a Step I calculation has been performed during the current time increment, then the time step Δt_{StepI} is determined in such a way that the maximum incremental deformation in the solid be equal to a user-prescribed value.

5. Application

This academic application intends to illustrate the added value of the proposed partitioned resolution, in the case of the filling and cooling of a parallelepipedic ingot (Figure 1). Liquid steel enters through the bottom inlet at prescribed temperature T_{fill} and velocity v_{fill}. Air is ejected at the top of the cavity during filling. Two symmetry planes are defined in $z = 0$ and 2.5 mm, making the problem planar (but analyzed in 3D). Heat is extracted from the metal through the metal/mould interface, using a convection-type expression for heat flux density: $q = h_T (T - T_{ext})$ where the heat transfer coefficient and the external temperature are constant. There is no heat flux between air and mould. The metal is supposed to stick along cavity walls.

5.1. Ingot filling

Figure 2 illustrates the filling sequence. The zero-isovalue of the level set function representing the metal/air interface is shown at various times, revealing waves and air entrapment caused by impingement against mould walls in the early stages of filling. As filling proceeds, the amplitude of waves at free surface reduces until the end of filling at time 1.72 s for which 80% of the cavity is
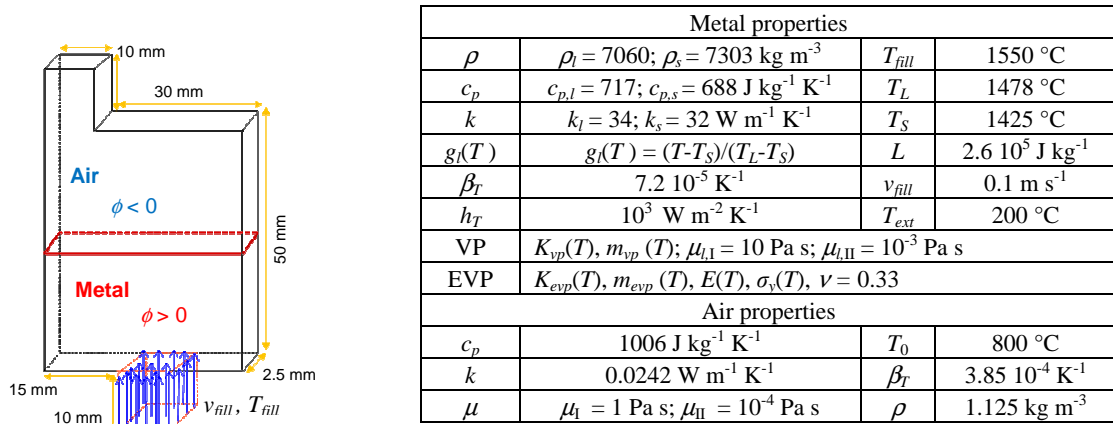
Figure 1: Definition of test case. Geometry and material properties.

	Metal properties		
ρ	$\rho_l = 7060;\ \rho_s = 7303$ kg m^{-3}	T_{fill}	1550 °C
c_p	$c_{p,l} = 717;\ c_{p,s} = 688$ J kg^{-1} K^{-1}	T_L	1478 °C
k	$k_l = 34;\ k_s = 32$ W m^{-1} K^{-1}	T_S	1425 °C
$g_l(T)$	$g_l(T) = (T-T_S)/(T_L-T_S)$	L	2.6 10^5 J kg^{-1}
β_T	7.2 10^{-5} K^{-1}	v_{fill}	0.1 m s^{-1}
h_T	10^3 W m^{-2} K^{-1}	T_{ext}	200 °C
VP	$K_{vp}(T),\ m_{vp}(T);\ \mu_{l,I} = 10$ Pa s; $\mu_{l,II} = 10^{-3}$ Pa s		
EVP	$K_{evp}(T),\ m_{evp}(T),\ E(T),\ \sigma_y(T),\ \nu = 0.33$		
	Air properties		
c_p	1006 J kg^{-1} K^{-1}	T_0	800 °C
k	0.0242 W m^{-1} K^{-1}	β_T	3.85 10^{-4} K^{-1}
μ	$\mu_I = 1$ Pa s; $\mu_{II} = 10^{-4}$ Pa s	ρ	1.125 kg m^{-3}

a) $t = 0.21$ s   b) $t = 0.56$ s   c) $t = 0.85$ s   d) $t = 1.72$ s, $v_{l,max} = 180$ mm/s, $\sigma_{yy,max} = 4.23$ MPa
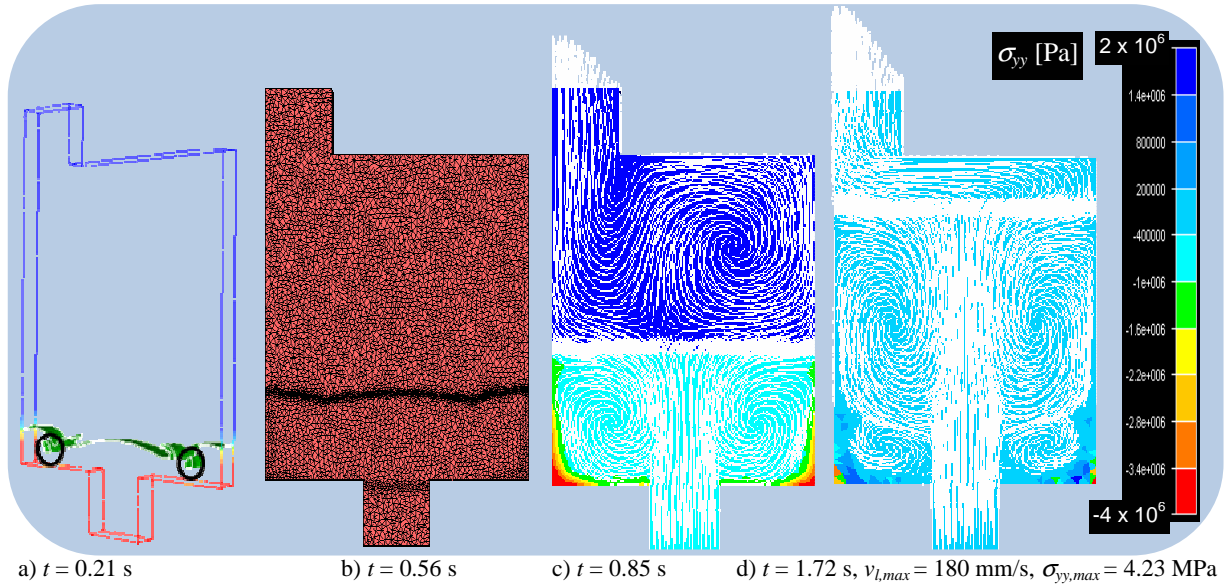
Figure 2: a) Free surface evolution in early stages of filling; b) adapted mesh during filling; c) fluid flow in metal and air, and solid fraction at mid-filling; d) fluid flow and vertical stress in solid shell at the end of filling.

filled. The Figure also shows mesh adaptation, fluid flow in terms of velocity vectors, together with the formation of stress in the solid shell during filling.

5.2. Ingot cooling

After filling, the ingot is cooled down under the same heat extraction conditions. At time 10 s, during solidification, the fluid flow and stresses in the solid are shown in Figure 3, using four different computational strategies. It can be seen in Figure 3a that a sole solid-oriented resolution (that is a resolution with an arbitrary high value of liquid viscosity, 10 Pa s) shows only a liquid feeding flow that compensates solidification shrinkage. Such a simulation gives access to stresses in solidified regions but is not representative of fluid flow. As shown in Figure 3b, this result can be improved by taking a lower viscosity value, 1 Pa s. However this value can be considered as the lower bound for such a formulation, and convection velocities are still too low.

In Figure 3c, the result of a sole liquid-oriented resolution is displayed. In such a resolution, the metal is considered as a non-Newtonian fluid whatever its temperature. As this formulation permits lower viscosity values, fluid flow is well modelled. The increase of the viscoplastic consistency when decreasing temperature gives rise to the freezing of solidified regions. However, stresses in these

solidified regions are null. Because of the fluid-like behaviour, deviatoric stresses are proportional to strain-rates: no flow, no stress!

Finally, Figure 3d illustrates the proposed partitioned solution scheme. It can be seen that both fluid flow and stresses can be correctly computed.

Comparing cases c and d with a and b, it can be seen that the calculation of fluid flow directly affects the extension of the solidified region and the shape of the metal free surface. This difference is due to the smoo-thing of temperature gradients in the liquid pool that results from fluid flow: we change from a diffusive regime when no flow, to a convective regime when natural convection is correctly modelled.

6. Conclusion

The proposed method demonstrates the feasibility of consistent and concurrent nume-rical resolution of fluid flow and solid mechanics. A future perspective is its implementa-tion in the solidification code Thercast®. This should provide an efficient tool for optimizing casting processes.
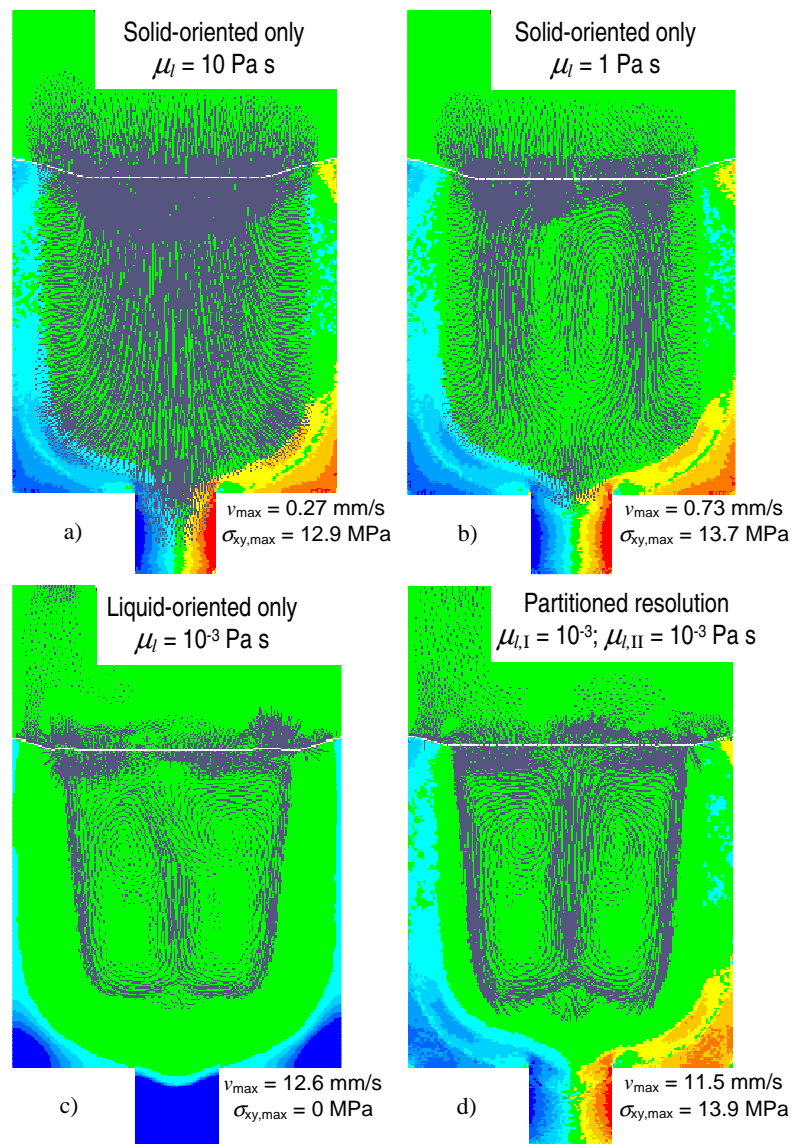

Figure 3: Four different results obtained by different formulations. Only the proposed partitioned scheme gives access to fluid flow and stresses in solid regions (shear stress represented here).

References
[1] Bellet M and Fachinotti V D 2004 *Comp. Meth. Appl. Mech. Eng.* **193** 4355-81
[2] Bellet M, Jaouen O and Poitrault I 2005 *Int. J. Num. Meth. Heat Fluid Flow* **15** 120-142
[3] Fachinotti V D and Cardona A 2007 *Int. J. Numer. Meth. Engng.* **70** 728-755
[4] Hamide M, Massoni E and Bellet M 2008 *Int. J. Num. Meth. Engng.* **73** 624-641
[5] Hughes T J R 1987 *Int. J. Num. Meth. Fluids* **7** 1261–75
[6] Ni J and Beckermann C 1991 *Metall. Trans.* B **22** 349-361
[7] Osher S and Sethian J 1988 *J. Comput. Physics* **79** 12-69
[8] Tezduyar T E and Osawa Y 2000 *Comp. Meth. Appl. Mech. Eng.* **190** 411-430
[9] Ville L, Silva L and Coupez T 2011 *Int. J. Num. Meth. Fluids* **66** 324-344